The use of circular optical grating for measuring angular rotation of mirrors

H.M. Shang, S.L. Toh, Y. Fu, C. Quan, C.J. Tay

Department of Mechanical Engineering, National University of Singapore, 10 Kent Ridge Crescent, Singapore 119260, Singapore

Abstract

This paper explores the feasible use of circular optical grating for measuring the rotation of mirrors that are commonly found in micro-systems. Both theoretical and experimental results show that distortion of the circular grating that is projected onto the mirror surface is a simple function of the angular rotation of the mirror. The circular grating may readily be generated using a standard Michelson interferometer or an LCD projector. Through manipulating the distance between the interferometer and the mirror surface, the diameter of the optical grating may be varied. Furthermore, the additional use of a converging lens enables a significant reduction in the size of the grating: with simple laboratory facility, small circular grating of about 400 μm is achieved for use on micro-systems. With the use of more sophisticated optical elements, the angular rotation of even smaller micro-mirrors may be measured.

Keywords: Circular optical grating; Micro-mirror

1. Introduction

Since the invention of the laser, optical measurement and inspection techniques for diffuse and specularly reflective surfaces using moiré, projected-fringes, laser triangulation with both point-light and line-light, holography, and shearography have entered a new dimension [1–19]. These traditional techniques were originally developed for use on large objects, but they are now being used on micro-electromechanical systems (MEMS) and thin-film structures [7–11, 20–23]. For example, linear-displacements and strains are measured using moiré [7–11], optical flat [20], holography [21–23] and grating interferometry [22], whereas angular rotations are measured using grating interferometry [10, 11], internal-reflection effects of prisms [24,25], laser speckles [26], Fabry–Perot interferometry [27] and other optical methods.

Small movable mirrors made from monocrystalline silicon are found in various commercial applications, for example, as multiple-mirror devices for projection displays in HDTV, and as beam deflection devices with mirror sizes ranging from about 100 μm to about 3 mm [28–30]. The angular-rotation of the mirror about its axis is often controlled through the application of electrical voltage. Among the existing measurement methods

for angle of rotation, such as those based on interferometry, internal-reflection of optical elements and others [1–19, 24–27], each has its advantages and limitations. For example, the method of point-of-light triangulation is easy to perform, requiring only a simple optical arrangement; but if the illuminating point lies on the axis of rotation, the angle of rotation of a diffuse surface cannot be determined unless three non-collinear illuminating points are used. In the method of line-of-light triangulation, the change in pitch of the grating lines that are projected onto the rotating surface is related to the rotating angle. However, the angle of rotation cannot be determined if the direction of the grating lines happens to be perpendicular to the axis of rotation. The use of a circular grating does not suffer from this drawback: the angular rotation of both diffuse and specularly reflective surfaces about any axis of rotation can be determined from the distortion of the grating. The main objective of this paper is to describe a simple method for measuring a small angle of rotation of a flat mirror using a circular optical grating. The distorted grating that is diffracted from the specularly reflective surface, or the mirror surface, may be recorded in two different ways using a CCD camera. In the first method, the distorted grating is recorded off the mirror surface as though it were a diffuse surface. In the second method, the distorted grating is specularly reflected onto an opaque screen and the CCD camera subsequently records the grating image off this screen.

Optical grating may be generated and projected onto a surface using an LCD projector or a Michelson interferometer (Fig. 1(a)), which is a typical example of the two point-light source techniques [1–5,31]. Unlike Michelson interferometers, LCD projectors are not always available in laboratories. With a Michelson interferometer, hyperbolic grating is observed on a flat screen when it is placed parallel to the line containing the two closely spaced point-light sources, whereas circular grating is observed when the screen is normal to the line containing the two point-light sources [31]. By placing an expander between the beam-splitting cube and the laser source and by carefully adjusting the two mirrors beside the beam-splitting cube (Fig. 1(a)), a circular grating such as that shown in Fig. 1(b) is observed on the screen. Close examination of Fig. 1(b) reveals that the grating is not perfectly circular; this is due to both the screen and the recording plane not being perpendicular to the direction of grating-projection [31].

With reference to Fig. 2, two point-light sources $S(0, 0, D)$ and $S'(0, 0, D + d_z)$ are located on the reference z-axis, which is normal to a flat screen placed in the xy-plane. As illustrated in Fig. 1(b), the resulting interference pattern that is observed on the screen thus comprises a family of concentric circles that satisfies the following expression [31].

$$x^2 + y^2 = \frac{(d_z^2 - \Delta^2)^2 + 4D(d_z^2 - \Delta^2)(D + d_z)}{4\Delta^2}, \tag{1}$$

where

$$\Delta = \frac{\lambda}{2}N \tag{2}$$

with λ denoting the wavelength of the laser source, and N denoting the fringe order (bright

fringes being labelled as even integers of N and dark fringes being labelled as odd integers of N). Thus, Eq. (1) may be perceived as the locus of a typical point, $P_0(x_0, y, 0)$ that lies on a fringe-circle of order N.

With reference to Fig. 1(a), adjusting the relative positions of the two mirrors beside the beam-splitting cube enables varying the amount of d_z and hence altering the pitch, or spacing, of these fringe-circles. Furthermore, with an additional converging lens placed between the beam-splitting cube and the screen (test surface), the size of the optical grating may be reduced to within a small area for use on micro-systems.

2. Theoretical considerations

2.1. Method I: Recording the distorted grating appearing on the mirror surface

As shown in Fig. 2, consider that the same interference pattern generated by point-light sources $S(0, 0, D)$and $S'(0, 0, D + d_z)$ and expressed by Eq. (1) is now projected onto a planar mirror surface that is inclined at the angle $\theta = \theta_1$. It is easily derived that the interference pattern appearing on the mirror surface is described by the following expression:

$$x^2 + y^2 = \frac{(d_z^2 - \Delta^2)^2 + 4D(d_z^2 - \Delta^2)(D + d_z)}{4\Delta^2} + \left[\frac{d_z^2 - \Delta^2}{\Delta^2}\right] Z^2 - \left[\frac{(d_z^2 - \Delta^2)(2D + d_z)}{\Delta^2}\right] Z, \tag{3}$$

where Δ is defined in Eq. (2), and Z, the z-coordinate of any point $P(x, y, Z)$ on an interference fringe that is observed on the inclined surface, is given as follows:

$$Z = x \tan\theta. \tag{4}$$

Thus, $P(x, y, Z)$ may be perceived as the corresponding point of $P_0(x_0, y, 0)$ in Fig. 2 because of rotating the mirror surface about the y-axis from $\theta = 0$ (the xy-plane) to $\theta = \theta_1$(the inclined plane).

Suppose that the image of the circular grating that appears on the mirror surface is recorded with a photographic film or a CCD camera whose direction of recording is parallel to the reference z-axis. For convenience, unit magnification factor is considered during recording. Then, the grating-image that is recorded off the surface will be expressed mathematically by Eq. (3) for $\theta \neq 0$ (inclined mirror) and by Eq. (1) for $\theta = 0$ (in the xy-plane).

In the following mathematical derivations, the mirror surface is considered to rotate slightly about the y-axis from the initial angle $\theta_1$to the angle θ_2. Subsequently, the circular grating is distorted only along the x-axis. Suppose that the length parallel to the

x-axis of a specific fringe-circle that appears on the xy-plane ($\theta = 0$) is denoted by $X = 2x_0$ and by Y in a direction parallel to the y-axis. The value of X is changed to X_1 and X_2 as θ attains the values θ_1 and θ_2, whereas the value of Y is unchanged throughout the angular change. As illustrated in Fig. 2, the same fringe-circle of a specific fringe order N (or a specific value of Δ) will intersect a plane parallel to the xz-plane at points $P_1(x_1, y, Z_1)$ and $P_1'(x_1', y, Z_1')$on the inclined mirror surface θ_1, and at points $P_2(x_2, y, Z_2)$ and $P_2'(x_2', y, Z_2')$ on the inclined mirror surface θ_2. These points will correspond to $P_0(x_0, y, 0)$ and$P_0' \times (-x_0, y, 0)$ along the x-axis on the planar surface when $\theta = 0$. Thus, for a given y-coordinate on the same fringe-circle appearing on the planes $\theta_1$and θ_2, the use of Eq. (3) yields the following relationship between the co-ordinates of $P_1(x_1, y, Z_1)$ and $P_2(x_2, y, Z_2)$.

$$x_2^2 - x_1^2 = \left[\frac{d_z^2 - \Delta^2}{\Delta^2}\right][(Z_2 + Z_1) - (2D + d_z)](Z_2 - Z_1). \tag{5}$$

For two distantly located but closely spaced point-light sources $S(0, 0, D)$ and $S' \times (0, 0, D + d_z)$, the value of d_z may be neglected when compared to the value of D. Furthermore, with a small angle of rotation of a small mirror, it is permissible to neglect the value of $(Z_1 + Z_2)$ when compared to $2D$. Thus, Eq. (5) may be simplified to the following expression:

$$Z_2 - Z_1 \approx -\left[\frac{x_2^2 - x_1^2}{2D\xi}\right] = -\frac{x_2^2}{2D\xi}\left[1 - \left(\frac{x_1}{x_2}\right)^2\right], \tag{6}$$

where ξ is defined as follows:

$$\xi = \frac{d_z^2 - \Delta^2}{\Delta^2}. \tag{7}$$

Small reflecting mirrors are used in micro-systems. For a small mirror rotated through a small angle, it is permissible to treat $\delta \equiv (x_2 - x_1)$ as a small quantity. Using binomial expansion and retaining only the first two terms of the series, use of the approximation $(x_1/x_2)^2 \approx [1 - 2\delta/x_2]$ is appropriate such that Eq. (6) is simplified to the following expression:

$$Z_2 - Z_1 \approx -\frac{x_2\delta}{D\xi}. \tag{8}$$

Substituting Eq. (4) into Eq. (8) and considering small quantities of δ, θ_1andθ_2, the following expression is obtained:

$$Z_2 - Z_1 \approx (\theta_2 - \theta_1)x_2. \tag{9}$$

Thus, combining Eqs. (8) and (9) gives the following relationship between the amount of distortion of the fringe-circle along the x-axis and the angle of rotation.

$$\theta_2 - \theta_1 \approx -\frac{\delta}{D\xi} = -\frac{(x_2 - x_1)\lambda^2 N^2}{D(\lambda^2 N^2 - 4d_z^2)} = -K(x_2 - x_1), \tag{10}$$

where $K \equiv 1/D\xi$ is defined as a sensitivity factor related to the optical arrangement for a given fringe order N.

In a similar manner, the change in co-ordinates of $P_1'(x_1', y, Z_1')$ and $P_2'(x_2', y, Z_2')$ due to rotation from θ_1 to θ_2 leads to the following expression that is similar to Eq. (10).

$$\theta_2 - \theta_1 \approx -K(x_2' - x_1'). \tag{11}$$

Experimentally, it is often convenient to measure the sizes X_1 and X_2 along the x-axis (i.e., $y = 0$ in Fig. 2) of the same fringe-circle observed on the mirror surfaces θ_1 and θ_2. Thus, with $X_1 = (x_1 + x_1')$ and $X_2 = (x_2 + x_2')$, the use of Eqs. (10) and (11) gives the following expression:

$$\theta_2 - \theta_1 = -\frac{K}{2}(X_2 - X_1). \tag{12}$$

The angular rotation $(\theta_2 - \theta_1)$ of a small mirror may therefore be determined from the measured amount of distortion $(X_2 - X_1)$ of the circular grating after the optical sensitivity factor K is obtained by calibration. In deriving Eq. (12), the camera image plane is considered to be parallel to the x-axis (direction of recording being normal to the xy-plane). In reality, the camera image plane may be inclined at an angle with the reference x-axis; but this would only modify the sensitivity factor K in Eq. (12) by a constant value related to the angle of inclination. Thus, it is permissible to use Eq. (12) regardless of the direction of recording.

2.2. Method II: Recording the reflected distorted grating off an opaque screen

The foregoing expressions (Method I recording) were derived for a grating-image that appears on the mirror surface as though it were a diffuse surface. When the grating-image is specularly reflected onto an opaque screen and its distorted image is subsequently recorded off this screen, the angle of rotation may also be determined from the distortion of the fringe-circle. As illustrated in Fig. 3, the optical grating is projected along the direction of the z-axis onto a specularly reflective surface that is inclined at the angle θ_1 with the reference x-axis. A fringe-circle of fringe order N is cast on the inclined surface so that, when it is specularly reflected by the surface, the length $P_1P_1'(\equiv X_1)$ of the distorted fringe-circle on the camera image plane (parallel to the x-axis) is now imaged as $P_3P_3'(\equiv X_1')$ on the camera image plane. It should be emphasised that in reality, because the grating that is generated and projected by the Michelson interferometer expands in size as it approaches the mirror surface, the reflected light rays P_1P_1 and $P_1'P_1'$ are not parallel, so are P_1P_3 and $P_1'P_3'$. Thus, the reflection angle between the light rays P_1P_3 and P_1P_1, and that between the light rays $P_1'P_3'$ and $P_1'P_1'$, is not equal to $2\theta_1$. However, for simplicity in the derivation, it is assumed that these reflection angles at P_1 and P_1' are equal to $2\theta_1$ as shown in Fig. 3 and that the size Y of the fringe-circle on the y-axis is unchanged. As will be seen later in Eq. (16), the use of this assumption will lead to a linear relationship

between rotational angle and grating distortion.

As before, a unit magnification factor is considered and the recording direction is assumed to be parallel with the reference z-axis. From geometry, the following expression may be derived:

$$X_1' \approx X_1(1 + 2\theta_1^2). \tag{13}$$

Consider now the mirror surface is rotated from θ_1 to θ_2 about the y-axis. The new length X_2 of the distorted fringe-circle that is cast on the surface is recorded as X_2'on the camera image plane. An expression similar to Eq. (13) for X_2'may also be derived and is shown as follows:

$$X_2' \approx X_2(1 + 2\theta_2^2). \tag{14}$$

Thus,

$$X_2' - X_1' \approx (X_2 - X_1) + 2(X_2\theta_2^2 - X_1\theta_1^2). \tag{15}$$

For a small mirror rotated through a small angle $(\theta_2 - \theta_1)$, the approximation $X_1\theta_1 \approx X_2\theta_2$may be invoked so that the $(X_2\theta_2^2 - X_1\theta_1^2)$-term in Eq. (15) may be ignored. Combining Eqs. (12) and (15), the following expression is obtained:

$$\theta_2 - \theta_1 \approx -\frac{K'}{2}(X_2' - X_1'), \tag{16}$$

where $K' \equiv 1/D_c\xi$ denotes the optical sensitivity, with ξ defined in Eq. (7).

As with Method I recording, the optical sensitivity factor K' in Eq. (16) is modified by a constant when the camera image plane is inclined at an angle with the reference x-axis; hence, the use of Eq. (16) is still appropriate.

From Eqs. (12) and (16), it is readily seen that, for both methods of recording, the angle of rotation of the mirror about the y-axis may be determined from the amount of distortion of the fringe-circle $(X_2 - X_1)$ or $(X_2' - X_1')$ that is measured off the image-plane of the CCD camera; the optical sensitivity factor K or K' may be obtained by calibration.

3. Experimental verification

A front-coated mirror is mounted on a rotating stage together with the optical setup shown in Fig. 1(a). The use of this mirror (approximately 10 mm by 10mm in size) does not undermine the eventual application of this technique because the minimum size of the micro-mirror, whose angular rotation is to be measured, is governed by the minimum size of the circular grating that can be generated. Fig. 1(b) shows a typical

circular grating that is recorded directly off the mirror surface (Method I recording) using a CCD camera—the diameter of the innermost circle is approximately 3.5mm and that of the fourth inner circle is approximately 8 mm. This infers that an optical grating of this size is suitable only for mirrors with the minimum size of 3.5-mm diameter. Table 1 shows the measured values of X (along the x-axis) and Y (along the y-axis) of the fourth inner circle. It is seen that the value of X changes with the angular orientation of the mirror whereas Y is unchanged, verifying that the mirror has rotated about its y-axis. The distortion $(X_2 - X_1)$of the fringe-circles along the x-axis, denoted by a dimensionless parameter $\psi(\equiv X_2 - X_1/Y_2)$, is plotted against the angular rotation and is shown in Fig. 4-the linear relationship enables the determination of the optical sensitivity factor K (Eq. (12)) to enable the subsequent use for measuring the angular rotation. Fig. 4 also shows a linear $[\psi \sim (\theta_2 - \theta_1)]$-relationship that is applicable to all other fringe-circles that appear in Fig. 1(b), implying that during measurement, the distortion of any fringe-circle may be used together with the same calibration curve.

With Method II recording, the optical grating projected on the mirror surface is reflected onto a flat opaque surface followed by recording its distorted image off the surface. Fig. 5 shows the linear relationship (described by Eq. (16)) between the distortion $\psi(\equiv X_2' - X_1'/Y_2')$of the fringe-circles and angular rotation. The spread in test results (Fig. 5) is grossly more severe than the spread in results obtained using Method I recording (Fig. 4). This is because, in deriving Eq. (16), the distortion along the y-axis is neglected and the reflection angle between the light rays $P_1P_3$and $P_1P_1$and that between the light rays $P_1'P_3'$and $P_1'P_1'$are each assumed to be $2\theta_1$, although, in reality, the grating propagates outwardly in a hyperbolic manner [31]. The data points in Fig. 5 seem to have suggested that a separate calibration curve is needed for each fringe-circle, even though they may be fitted with a single straight line. Finally, it should be mentioned that the results (not shown in this paper) have indicated that the scatter may be more severe with multiple reflection of the distorted grating before its image is finally cast on the opaque surface for recording.

It is obvious that the size of the rotating mirror cannot be smaller than the diameter of the innermost fringe-circle, which, as shown in Fig. 1(b), is approximately 3.5-mm diameter. For use in micro-systems where mirrors in the sub-micron range are used, the diameters of the fringe-circles may be reduced by means of a converging lens that is placed between the beam-splitting cube and the test surface (see Fig. 1(a)). Fig. 6 shows a typical circular grating whose innermost fringe-circle (outside the central dark-patch) on the mirror surface has been shrunk to approximately 400 μm in diameter. The linear relationships between grating distortion and rotation angle that are constructed using Method I and Method II recordings are shown in Fig. 7(a) and 7(b), respectively. In both figures, the following are observed: (a) the straight-line graphs do not pass through the origin, disagreeing with the prediction in Eqs. (12) and (16); and (b) a separate calibration graph is necessary for each fringe-circle. These observations may be attributed to the center of the projected circles not being coincident with the center of rotation of the mirror surface, thereby resulting in an effect that is equivalent to pure translation in addition to pure rotation of the mirror. This effect, therefore, necessitates the inclusion of a correction term in Eqs. (12) and (16). For simplicity, Eqs. (12) and (16) may simply be rewritten as follows:

$$\theta_2 - \theta_1 = \Gamma\psi + \Omega, \tag{17}$$

where Γ is related to the optical arrangement, and Ω is a correction term. Reflection will show that the experimental results in Figs. 4 and 5 may also be interpreted in the light of Eq. (17) with $\Omega \approx 0$.

4. A simple procedure for measuring angular rotation of micro-mirrors

Based on the foregoing experimental observations, the following simple procedure may be adopted for measuring the angular rotation of micro-mirrors. The optical system is first calibrated by mounting the micro-mirror on a rotating stage so that the distortion ψ of the grating corresponding to each angle of rotation $(\theta_2 - \theta_1)$ is measured; the constants Γ and Ω are determined from the slope and intercept of the $(\theta_2 - \theta_1) \sim\psi$ graph. Subsequently, when an electrical voltage is applied to the micro-mirror, the distortion of the grating enables the determination of the amount of angular rotation of the micro-mirror using Eq. (17) and the known values of Γ and Ω.

5. Conclusion

In this paper, a simple method is developed for the measurement of a small angle of rotation of a mirror using a circular optical grating. The grating may be generated and projected onto the mirror surface using a standard Michelson interferometer or an LCD projector. Due to its availability in most laboratories, a Michelson interferometer is described in this paper. As the angle of rotation is determined from the amount of distortion of the grating, the diameter of the innermost fringe-circle governs the minimum size of the mirror that can be used. Significant reduction in the optical grating diameter may be achieved with the additional use of a converging lens placed between the interferometer and the mirror. This paper has demonstrated that, with simple laboratory facility, the grating diameter of approximately 400 μm is easily achieved. Hence, the minimum size of the mirror that can be used is also 400 μm. With the use of sophisticated optical elements and the appropriate magnification, grating size suitable for even smaller mirrors may be generated. Present experimental results have shown a linear relationship between the amount of distortion of the fringe-circle and the angle of rotation: this is in agreement with that predicted by theory. Thus, after calibration, the optical system may be used for measuring small angles of rotation of micro-mirrors.

References

[1] Collier RJ, Burckhardt CB, Lin LH. Optical holography. New York: Academic Press, 1971.

[2] Erf RK. Holographic nondestructive testing. New York: Academic Press, 1971.

[3] Vest CM. Holographic interferometry. New York: Wiley, 1979.

[4] Ostrovsky YI, Butusov MM, Ostrovskaya GV. Interferometry by holography. New York: Springer, 1980.

[5] Jones R, Wykes C. Holographic and speckle interferometry - a discussion of the theory, practice and application of the techniques. Cambridge: Cambridge University Press, 1989.

[6] Dally JW, Riley WF. Experimental stress analysis. 2nd ed. New York: McGraw Hill, International Student Edition, 1978.

[7] Post D, Han B, Ifju P. High sensitivity Moiré - experimental analysis for mechanics and materials. Berlin: Springer, 1994.

[8] Rastogi PK, editor. Optical measurement techniques and applications. USA: Artech House, 1997.

[9] Rastogi PK, Inaudi D, editor. Trends in optical nondestructive testing and inspection, UK: Elsevier Press, 2000.

[10] Ligtenberg FK. The Moiré method, a new experimental method for determining moments in small slab models. Proc Soc Exp Stress Anal 1954;12(2):83-98.

[11] Kao TY, Chiang FP. Family of grating techniques of slope and curvature measurements for static and dynamic flexure of plates. Opt Eng 1982;21(4):721-42.

[12] Ennos AE, Virdee MS. High accuracy profile measurement of quasi-conical mirror surface by laser autocollimation. J Prec Eng 1982;4:5-8.

[13] Rastogi PK. An electronic pattern speckle shearing interferometer for the measurement of surface slope variations of three-dimensional objects. Opt Lasers Eng 1997;26(2-3):93-100.

[14] Huang JR, Ford HD, Tatam RP. Slope measurement by two-wavelength electronic shearography. Opt Lasers Eng 1997;27(3):321-33.

[15] Leendertz JA, Butters JN. An image shearing speckle pattern interferometer for measuring bending moments. J Phys 1974;7:168-72.

[16] Hung YY. Shearography: a new optical method for strain measurement and nondestructive testing. Opt Eng 1982;21(3):391–95.

[17] Hung YY, Lin L, Shang HM. 3-D machine-vision technique for rapid 3D shape measurement and surface quality inspection. In: SAE Technical Paper Series 1999-01-0418. 1999 SAE International Congress and Exposition, Society of Automotive Engineering, March 1–4, 1999, Cobo Center, Detroit, MI, USA.

[18] Hung YY, Lin L, Shang HM, Park BG. Practical 3D computer vision techniques for full-field surface measurement. Opt Eng 2000;139(1):143–9.

[19] Hung YY, Shang HM. Nondestructive inspection of specularly reflective objects using a reflective 3D computer vision technique. In: Paper No. 213. 1999 SEM Spring Conference and Exposition on Theoretical, Experimental and Computational Mechanics, Society of Experimental Mechanics, June 7–9, 1999, Cincinnati, Ohio, USA.

[20] Zhang LY, Qin S, Shang HM. An optical study of the mechanical behavior of the micro-beam of an accelerometer. Proceedings of the Fourth International Conference on Composites Engineering, Hawaii, USA, 6–12 July 1997. p. 877–878.

[21] Jüptner W, Seebacher S, Osten W. Digital holography as a versatile tool for the investigation of the material behavior of micro components. Proceedings of the International Conference on Advanced Technology in Experimental Mechanics, Wakayama, Japan, JSME-MMD, 1997. p. 415–418.

[22] Jüptner W, Kujawinska M, Osten W, Salbut L, Seebacher S. Combined measurement of silicon microbeams by grating interferometry and digital holography. Proc SPIE 1998;3407:348–57.

[23] Seebacher S, Baumbach Th., Osten W, Jüptner W. Combined measurement of shape and deformation of small objects using digital holographic contouring and holographic interferometry. Proc International Conference on Trends in Optical Non-Destructive Testing, Lugano, Switzerland, 3–5 May, 2000.

[24] Huang PS, Kiyono S, Kamada O. Angle measurement based on the internal-reflection effect: a new method. Appl Opt 1992;31(28):6047–55.

[25] Huang PS, Li Y. Small-angle measurement by use of a single prism. Appl Opt 1998;37(28):6636–42.

[26] Tiziani HJ. A study of the use of laser speckle to measure small tilts of optically rough surfaces. Opt Communi. 1972;5(4):271–6.

[27] Kiang MH, Solgaard O, Muller RS, Lau KY. Silicon-micromachined micromirrors with integrated high-precision actuators for external-cavity semiconductor lasers. IEEE Photon Technol Lett 1996;8(1):95–7.

[28] Lang W, Pavlicek H, Marx Th., Scheithauer H, Schmidt B. Electrostatically actuated micromirror devices in silicon technology. Sensors Actuators A 1999;74:216–8.

[29] Sampsell JB. The digital micromirror device, its applications to projection displays. Journal of Vacuum Science & Technology B, Nov–Dec 1994;12(6):3242–6.

[30] Gessner T, Dotzel W, Billep D, Hahn R, Kaufmann C. Silicon mirror arrays fabricated by using bulk- and surface micromachining. Proc SPIE 1997;3008:34.

[31] Shang HM, Quan C, Tay CJ, Hung YY. Generation of carrier fringes in holography and shearography. Appl Opt 2000;39(16):2638-45.

List of Table

List of Figures

Angle θ (deg)	X (pixels)[a]	Y (pixels)[a]	ψ
$\theta_1 = 0$	$X_1 = 296$	$Y_1 = 277$	—
$\theta_2 = 0.5$	$X_2 = 298$	$Y_2 = 277$	0.0072
1.0	300	277	0.0144
1.5	302	277	0.0217
2.0	305	278	0.0324
2.5	311	280	0.0536
3.0	311	277	0.0542
3.5	313	277	0.0614
4.0	316	277	0.0722
4.5	318	276	0.0797
$\theta_2 = 5.0$	$X_2 = 320$	$Y_2 = 277$	0.0866

[a] Length scale is 34 pixels/mm.

Table 1

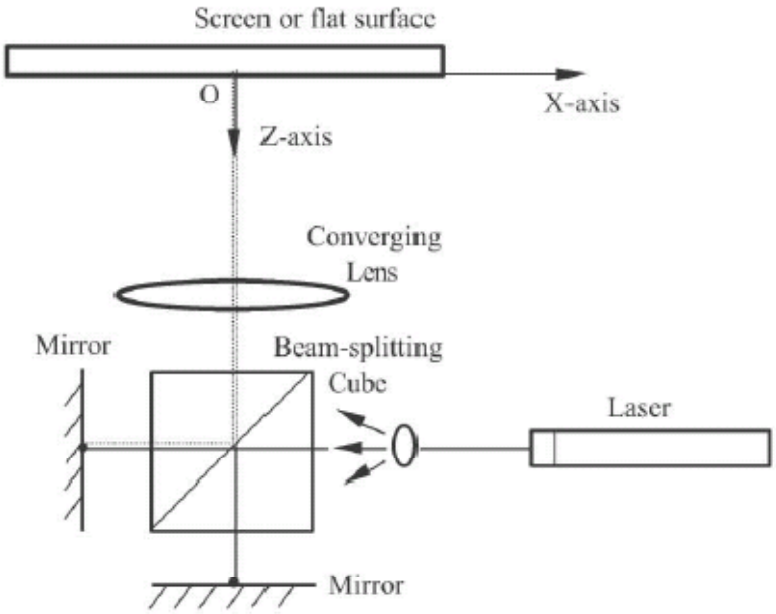
Screen or flat surface
O
X-axis
Z-axis
Converging
Lens
Mirror
Beam-splitting
Cube
Laser
Mirror

(a)

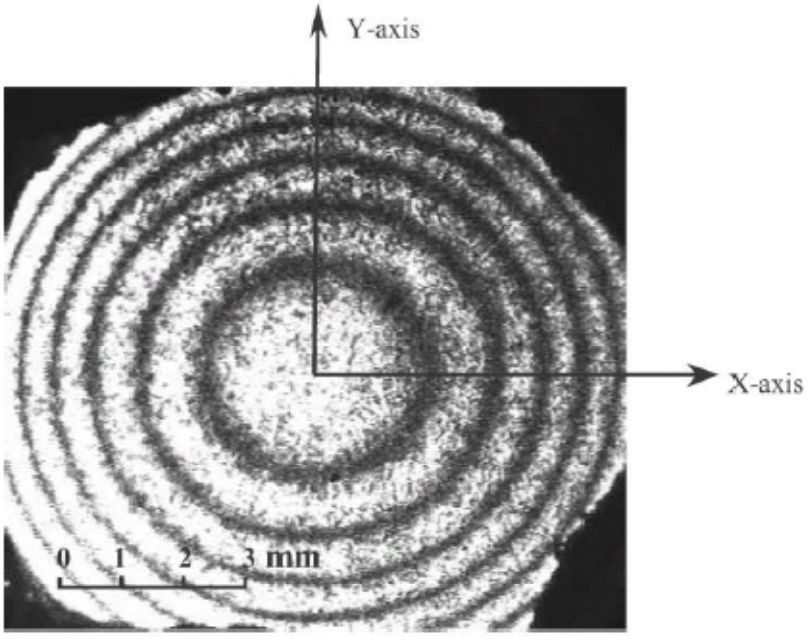
Y-axis
X-axis
0 1 2 3 mm

(b)

Fig. 1

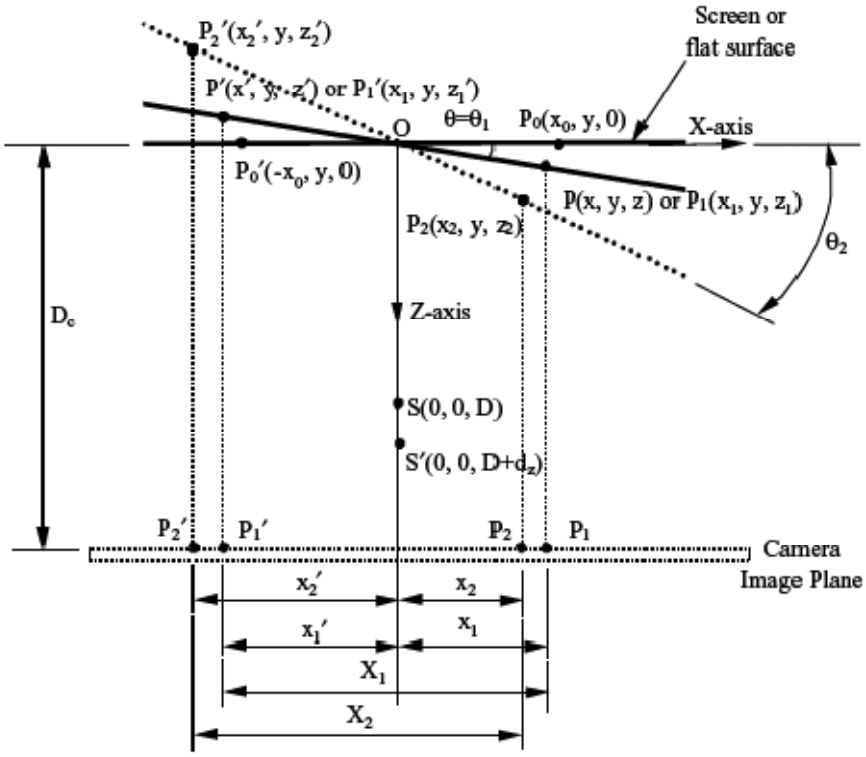
$P_2'(x_2', y, z_2')$
Screen or
flat surface
$P'(x', y, z')$ or $P_1'(x_1, y, z_1')$
$\theta=\theta_1$
$P_0(x_0, y, 0)$
X-axis
O
$P_0'(-x_0, y, 0)$
$P(x, y, z)$ or $P_1(x_1, y, z_1)$
$P_2(x_2, y, z_2)$
θ_2
D_c
Z-axis
$S(0, 0, D)$
$S'(0, 0, D+d_z)$
P_2'
P_1'
P_2
P_1
Camera
Image Plane
x_2'
x_2
x_1'
x_1
X_1
X_2

Fig. 2

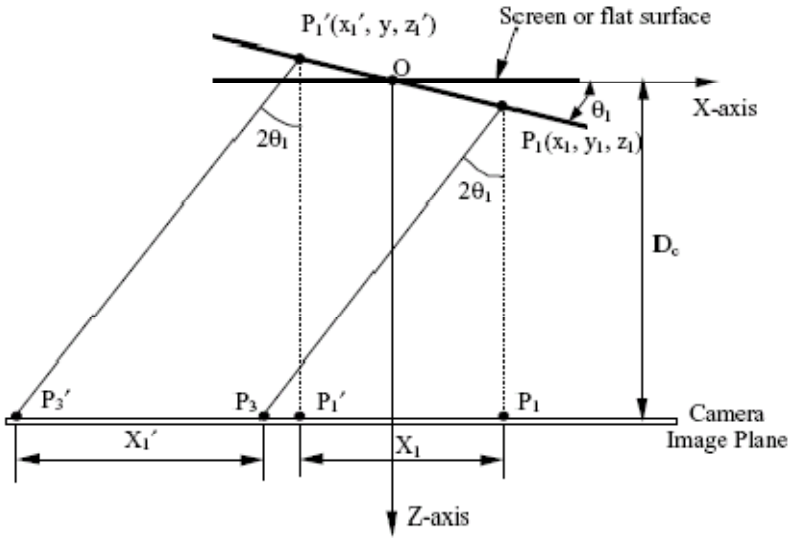
P1′(x1′, y, z1′)
Screen or flat surface
O
X-axis
θ1
2θ1
P1(x1, y1, z1)
2θ1
Dc
P3′
P3
P1′
P1
Camera
Image Plane
X1′
X1
Z-axis

Fig. 3

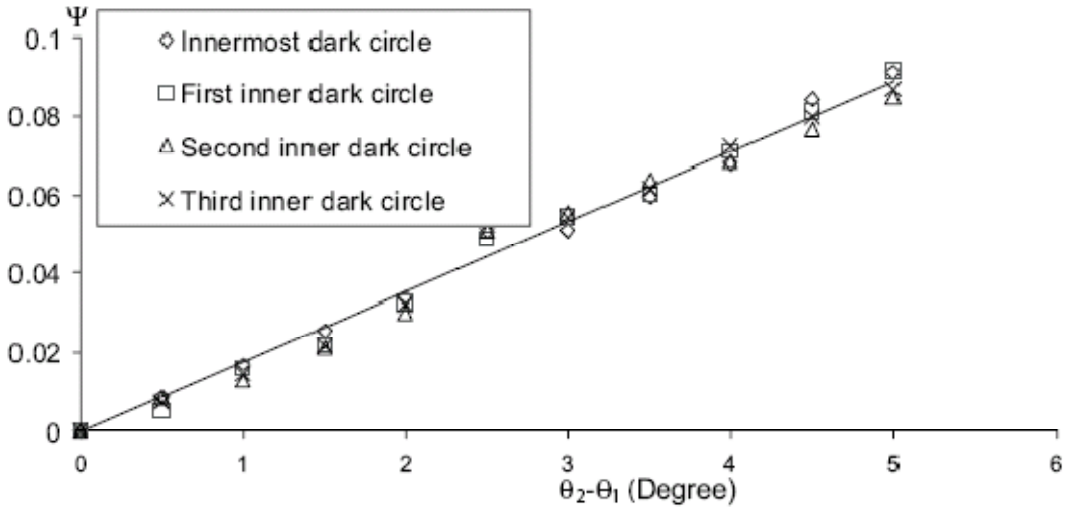
Ψ
0.1
0.08
0.06
0.04
0.02
0
Innermost dark circle
First inner dark circle
Second inner dark circle
Third inner dark circle
0
1
2
3
4
5
6
θ2-θ1 (Degree)

Fig. 4

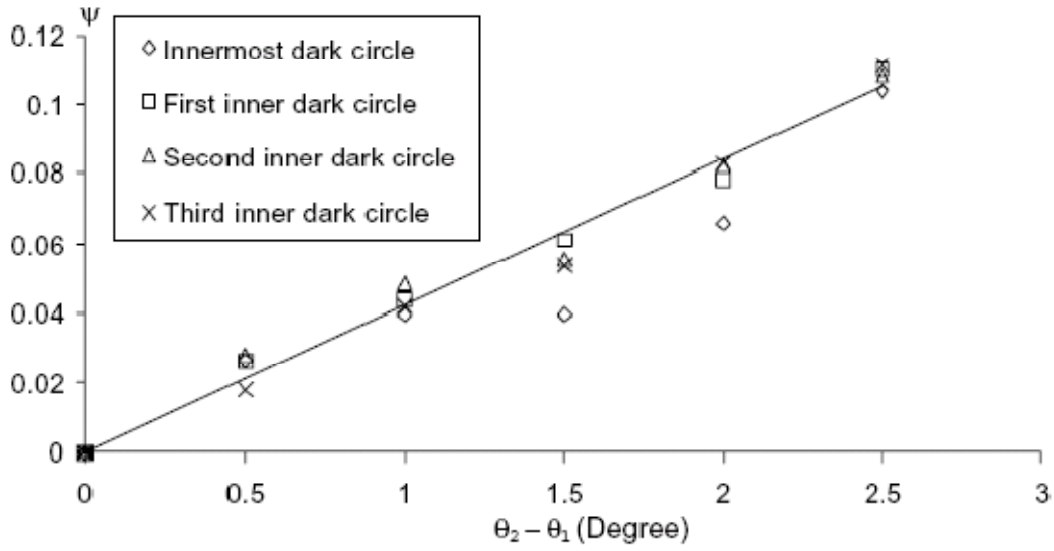
ψ
0.12
0.1
0.08
0.06
0.04
0.02
0
Innermost dark circle
First inner dark circle
Second inner dark circle
Third inner dark circle
0
0.5
1
1.5
2
2.5
3
θ2 – θ1 (Degree)

Fig. 5

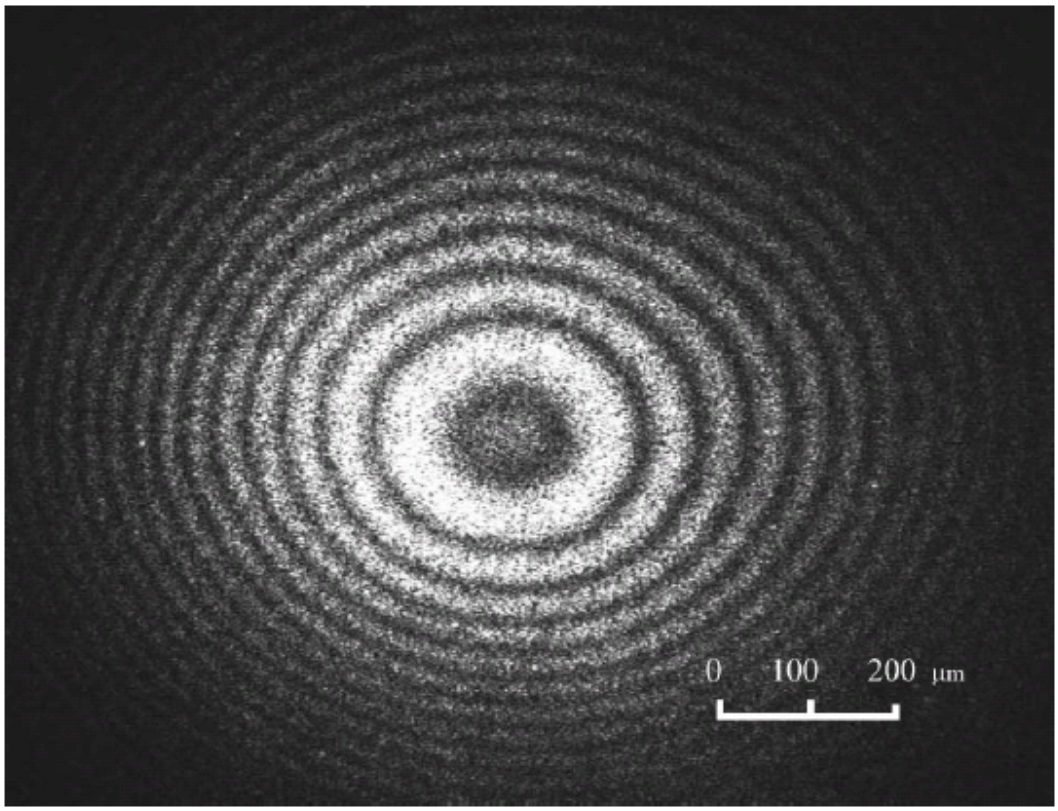

Fig. 6

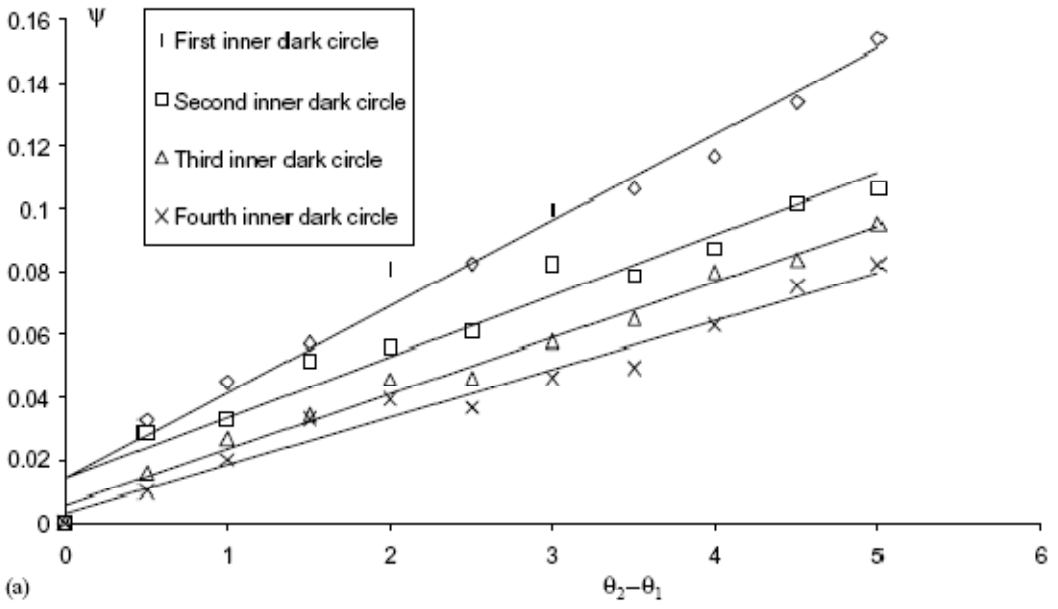
ψ
First inner dark circle
Second inner dark circle
Third inner dark circle
Fourth inner dark circle
0.16
0.14
0.12
0.1
0.08
0.06
0.04
0.02
0
0
1
2
3
4
5
6
θ2−θ1
(a)

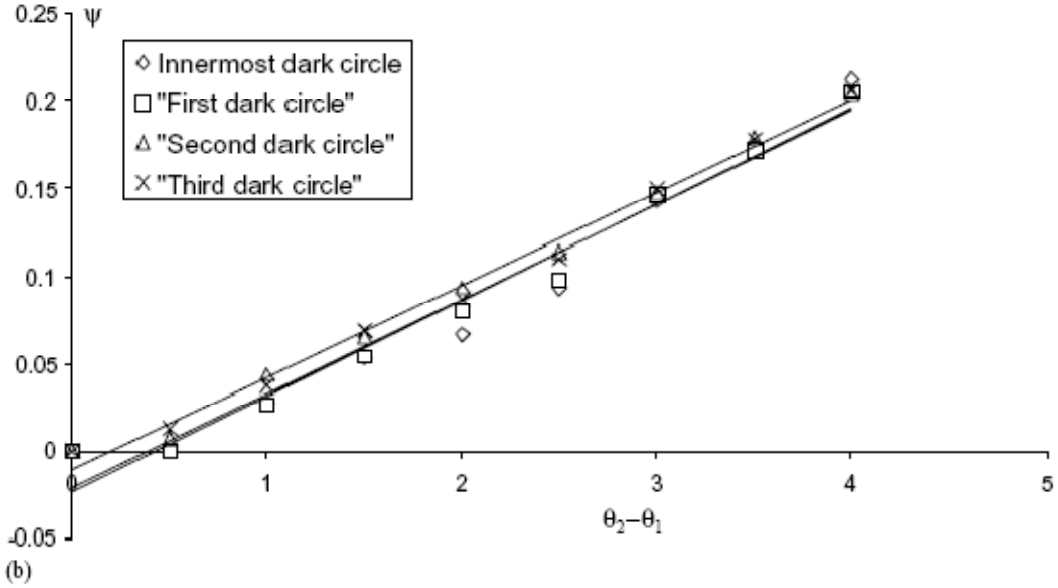
ψ
Innermost dark circle
"First dark circle"
"Second dark circle"
"Third dark circle"
0.25
0.2
0.15
0.1
0.05
0
-0.05
1
2
3
4
5
θ2−θ1
(b)

Fig. 7